

PLANT SCIENCE

Apoplastic barriers are essential for nodule formation and nitrogen fixation in *Lotus japonicus*

Defeng Shen¹, Nikola Micic², Rafael E. Venado³, Nanna Bjarnholt², Christoph Crocoll², Daniel Pergament Persson², Sebastian Samwald^{1,4}, Stanislav Kopriva^{4,5}, Philip Westhoff⁴, Sabine Metzger^{4,5}, Ulla Neumann¹, Ryohei Thomas Nakano^{1†}, Macarena Marín Arancibia³, Tonni Grube Andersen^{1,4*}

Establishment of the apoplastic root barrier known as the Casparian strip occurs early in root development. In legumes, this area overlaps with nitrogen-fixing nodule formation, which raises the possibility that nodulation and barrier formation are connected. Nodules also contain Casparian strips, yet, in this case, their role is unknown. We established mutants with defective barriers in *Lotus japonicus*. This revealed that effective apoplastic blockage in the endodermis is important for root-to-shoot signals underlying nodulation. Our findings further revealed that in nodules, the genetic machinery for Casparian strip formation is shared with roots. Apoplastic blockage controls the metabolic source-sink status required for nitrogen fixation. This identifies Casparian strips as a model system to study spatially constrained symbiotic plant-microbe relationships.

In vascular plants, barriers in the root endodermis force solute uptake to occur across the plasma membrane through active transport (1). This filtering mechanism emerges through the blocking of cross-cellular diffusion in the apoplast by localized lignin deposits known as Casparian strips (CS) (1). CS establishment coincides with protoxylem differentiation and root hair elongation (2). In legumes, the formation of symbiotic nodules—capable of fixing atmospheric nitrogen—is restricted to a similar narrow region known as

the susceptible zone (3). In the nonnodulating model plant *Arabidopsis thaliana* (hereafter *Arabidopsis*), the CS has been implicated in root-shoot nitrogen (N) response transduction (4). In nodulating model species, such as *Medicago truncatula* (hereafter *Medicago*) and *Lotus japonicus* (hereafter *Lotus*), nodule formation is tightly regulated by N availability. This occurs through a systemic signaling system called the autoregulation of nodulation network (AON) (5, 6). The AON ensures that under low-N conditions, expression of *C-TERMINALLY ENCODED*

PEPTIDE1 (*CEP1*) is induced in the root stele (7), and CEP1 peptides are translocated to the shoot and perceived by the COMPACT ROOT ARCHITECTURE2 (*CRA2*) receptor (8, 9). Once activated, *CRA2* receptors induce production of phloem-mobile signals known as CEP DOWNSTREAM1 and -2 (*CEPD1* and -2) (10). Besides this, *CRA2* also promotes synthesis of microRNA2111 (*miR2111*), which translocates from shoots to roots to repress the nodulation inhibitor *TOO MUCH LOVE* (*TML*) posttranscriptionally (10, 11). Thus, the AON allows the shoot to ensure that nodules only form when the root cannot obtain sufficient N from the surrounding soil (5, 6).

Anatomically, nodules are primarily derived from root cortex cells (12) but must connect to the vasculature across the endodermis. Therefore, the zonal co-occurrence with the endodermis-residing CS implies a connection between these developmental processes. Moreover, within the mature nodule, vascular bundles are also surrounded by endodermal cells that contain CS in their cell walls (13). Yet, it is unclear whether the exchange of fixed N and photosynthates

¹Max Planck Institute for Plant Breeding Research, Cologne, Germany. ²Department of Plant and Environmental Sciences, University of Copenhagen, Frederiksberg, Denmark. ³Genetics, Faculty of Biology, LMU Munich, Martinsried, Germany. ⁴Cluster of Excellence on Plant Sciences (CEPLAS), Düsseldorf, Germany. ⁵Institute for Plant Sciences, University of Cologne, Cologne, Germany.
*Corresponding author. Email: tandersen@mpipz.mpg.de
†Present address: Faculty of Science, Hokkaido University, Sapporo, Japan.

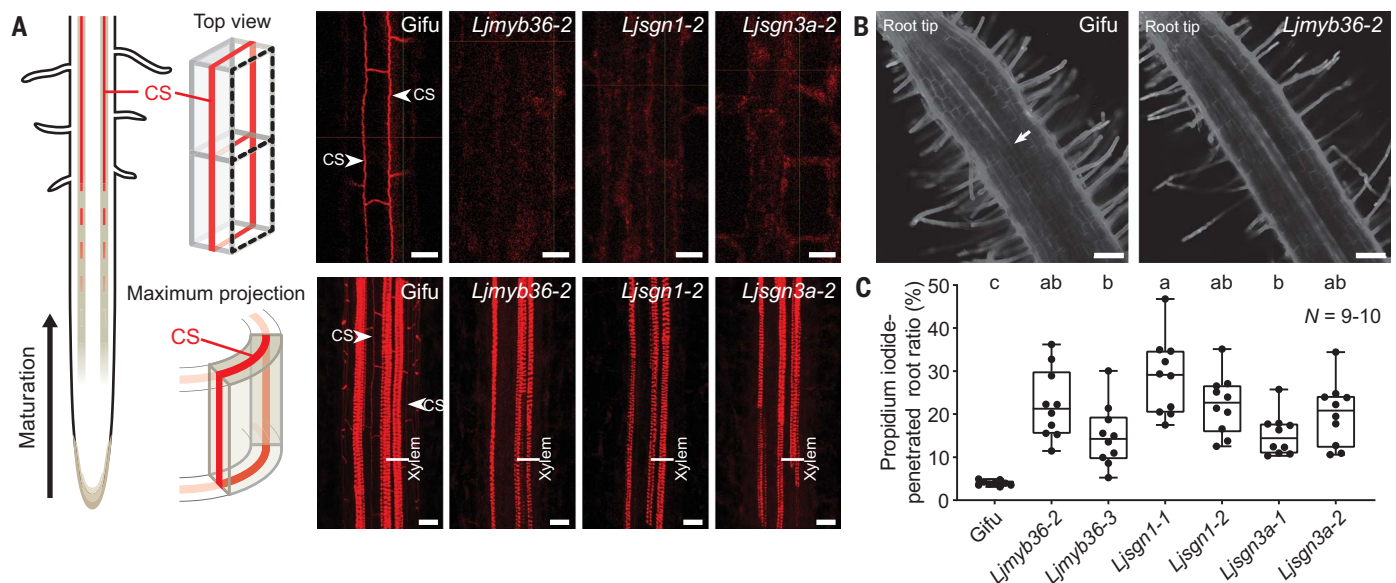


Fig. 1. Characterization of *Lotus* CS-defective mutants. (A) Top view (top) and maximum projection (bottom) of confocal image stacks of basic fuchsin-stained 9-day-old Gifu, *Ljmyb36-2*, *Ljsgn1-2*, and *Ljsgn3a-2* roots at a similar region. Arrowheads indicate CS. One of the xylem cell files is highlighted by a line. Representative images from three independent experiments ($N = 18$). (B) Representative images of propidium iodide (PI)-stained 9-day-old Gifu and *Ljmyb36-2* roots.

The arrow indicates the blockage of PI penetration into the vascular bundle. (C) Quantification of the proportion of 9-day-old roots that can be penetrated by PI into the vascular bundle. Representative results from two independent experiments. Different letters indicate statistically significant differences in a one-way analysis of variance (ANOVA) analysis with Tukey's test ($P < 0.05$). The number of biological replicates is indicated on the graph. Scale bars, 20 μm (A) and 100 μm (B).

between symbionts and the nodule vasculature is subject to apoplastic regulation. In this work, we address these questions using *Lotus* mutants with defective root and nodule apoplastic blockage to examine the role of CS in systemic signaling, nodule establishment, and function.

The genetic network underlying CS formation is conserved in *Lotus*

In *Arabidopsis*, CS establishment is controlled by the R3R2 MYB-class transcription factor MYB36 (14, 15) and facilitated by the leucine-rich repeat receptor-like kinase (LRR-RLK) SCHENGEN3/GASSHO1 (SGN3/GSO1) (16, 17) and the downstream receptor-like cytoplasmic kinase SCHENGEN1 (SGN1/PBL15) (18). We identified putative orthologs of each of these *Arabidopsis* genes in *Lotus*: *LjMYB36*, *LjSGN1*, *LjSGN3a*, and *LjSGN3b* (fig. S1A and table S1).

We obtained two independent homozygous *LOTUS RETROTRANSPOSON 1 (LOREI)* knock-out (KO) mutant lines for each of these, except *LjSGN3b* (table S2) (19, 20). *LjSGN3b* homozygous mutants may be nonviable, which would be consistent with *AtSGN3*'s role in *Arabidopsis* embryo development (21). In support of a CS-related function, the promoter regions of *LjMYB36*, *LjSGN1*, and *LjSGN3a* were active in the differentiation zone concurrent with the establishment of CS (fig. S1B). The wild-type (WT) accession Gifu (background of *LOREI* mutants) and all genotyped WT sibling plants of each mutant allele showed lignin-specific staining of xylem and CS as early as the susceptible zone, consistent with barrier establishment in this area. However, in all confirmed KO mutants, we observed only xylem-associated lignin signals (Fig. 1A and fig. S1C), and these plants had de-

layed blockage of the apoplastic tracer propidium iodide into the stele (22) (Fig. 1, B and C, and fig. S1D). Roots expressing the genomic sequence of *LjMYB36* or coding sequence of *LjSGN1* and *LjSGN3a* driven by their native promoter and untranslated regions showed complemented CS formation in the respective mutant backgrounds (fig. S1E). We therefore concluded that these mutations are causal for the defective CS formation. A transcriptome analysis of *Ljmyb36-2* and *Ljsgn3a-2* roots additionally revealed that genes involved in CS formation [e.g., *CASPARIAN STRIP DOMAIN PROTEINS (CASPs)* (23) and *ENHANCED SUBERIN 1 (ESB1)* (24)] were among the significantly down-regulated genes [false discovery rate (FDR)-adjusted $P < 0.05$] in CS mutants when compared with Gifu (fig. S2A and data S1). Thus, *LjMYB36*, *LjSGN1*, and *LjSGN3a* are all essential for CS formation in

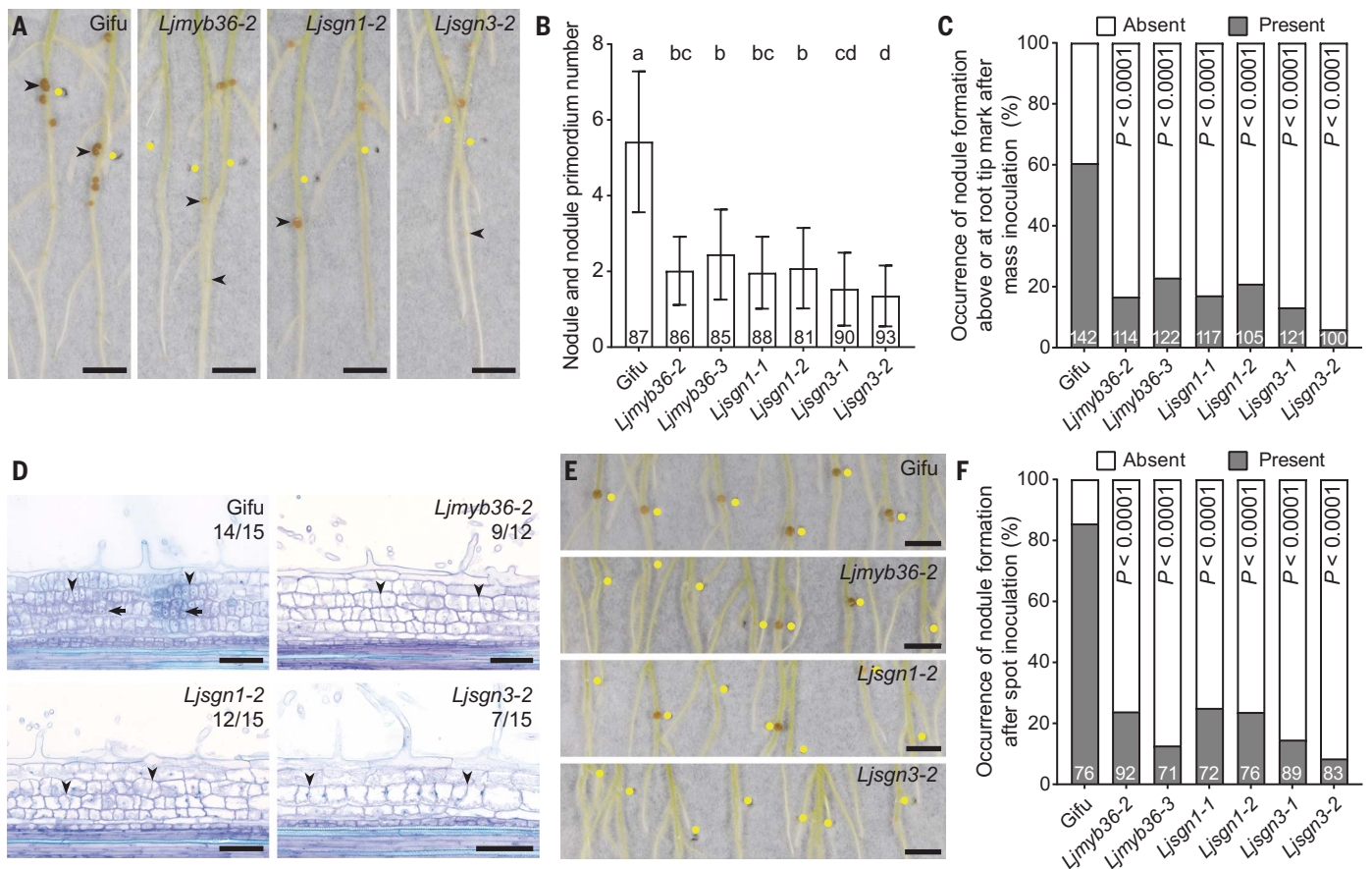


Fig. 2. Nodule formation is disturbed in CS-defective mutant roots.

(A) Representative images of mass-inoculated roots with nodules at 21 dpi. Arrowheads indicate the first nodule formed on the primary root. Yellow dots indicate the position of the primary root tip at 0 dpi. (B) Quantification of nodule and nodule primordium number at 21 dpi after mass inoculation. Combined results from three independent experiments. Error bars represent SDs. Different letters indicate statistically significant differences in a one-way ANOVA analysis with Tukey's test ($P < 0.05$). (C) Quantification of occurrence of nodule formed above or at the root tip position marked at 0 dpi after mass inoculation. Combined results from four independent experiments. P values

indicate Fisher's exact test (comparison with Gifu). (D) Representative images of semithin sections on nodule primordia at 3 dpi after spot inoculation. Numbers on the graph indicate proportion of root segments with shown mitotic activity. Arrowheads and arrows indicate anticlinal and periclinal divisions induced in the cortex, respectively. (E) Representative images of spot-inoculated roots at 14 dpi. Yellow dots indicate the position of spot inoculation at 0 dpi. (F) Quantification of occurrence of nodule formation at 14 dpi after spot inoculation. Combined results from three independent experiments. P values indicate Fisher's exact test (comparison with Gifu). The number of biological replicates is indicated on the graph. Scale bars, 5 mm [(A) and (E)] and 100 μ m (D).

Lotus roots, and *LjSGN3a* was termed *LjSGN3* for consistency with other species.

CS establishment is central for nodule initiation and development

Upon inoculation with the symbiont *Mesorhizobium loti* R7A, nodule occurrence was

significantly reduced on *Ljmyb36*, *Ljsgn1*, and *Ljsgn3* roots compared with Gifu and their respective WT sibling lines (Fig. 2, A and B, and fig. S3A). In Gifu plants, the first nodule on the primary root (Fig. 2A, arrowheads) occurred close to or at the root tip position marked at 0 days postinoculation (dpi) (Fig. 2A, yellow

dots). Yet, this happened less frequently in CS mutants (6 to 23%), indicating a delayed nodule formation (Fig. 2, A and C). Despite unaffected rhizobial abundance on root surfaces at the initial stage (1 dpi) (fig. S3B), these mutants displayed a significant reduction in infection thread density and nodule size and

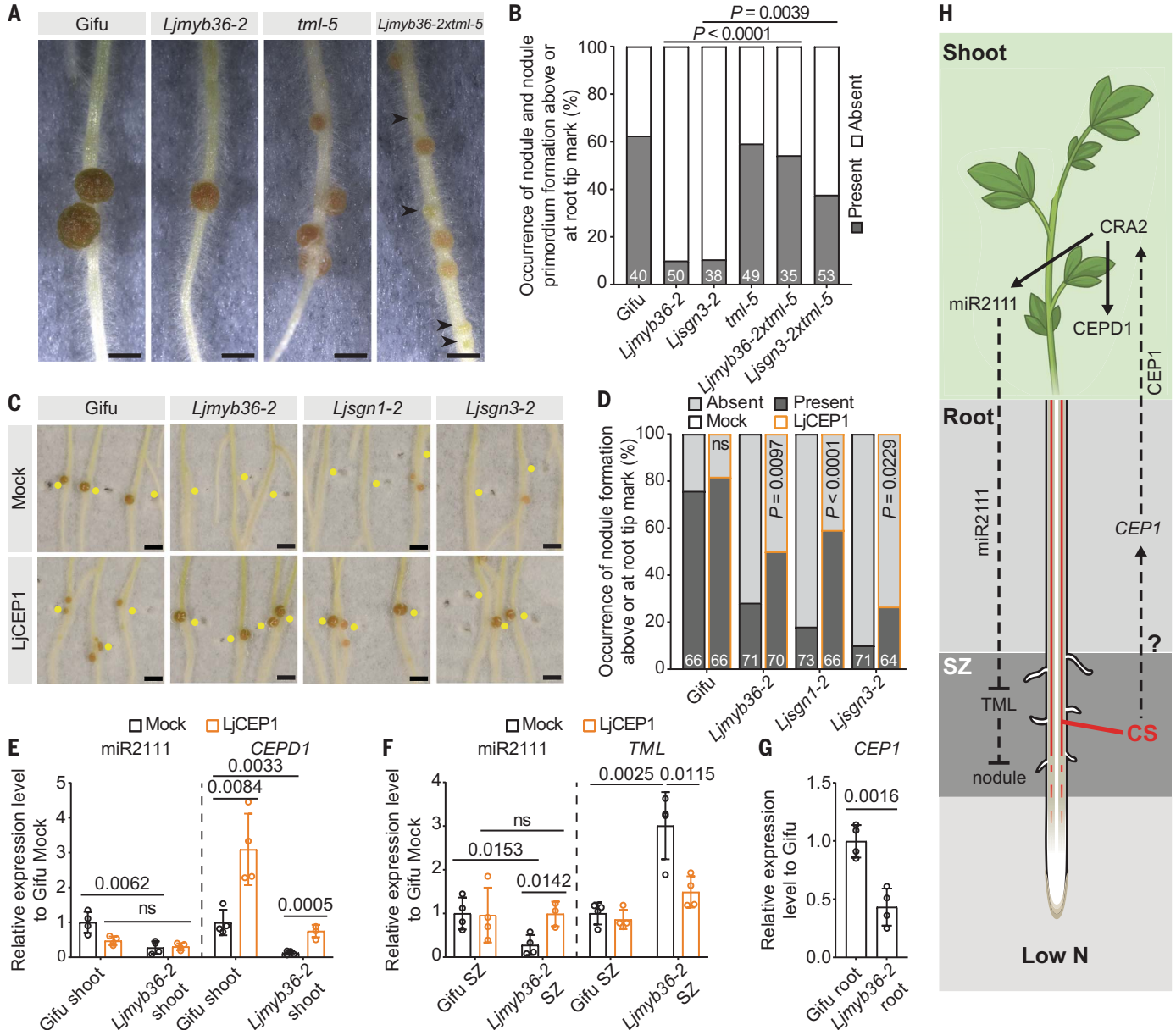


Fig. 3. Disturbed nitrogen signaling leads to reduced nodule formation in CS-defective mutant roots.

(A) Representative images of mass-inoculated roots with nodules at 28 dpi. Arrowheads indicate nodule primordia. (B) Quantification of occurrence of nodule and nodule primordium formed above or at the root tip position marked at 0 dpi after mass inoculation. Combined results from two independent experiments. P values indicate Fisher's exact test. (C) Representative images of mass-inoculated roots treated with mock (water) or 1 μ M LjCEP1 at 21 dpi. Yellow dots indicate the positions of the primary root tips at 0 dpi. (D) Quantification of occurrence of nodule primordium formed above or at the root tip position marked at 0 dpi after mass inoculation. P values indicate Fisher's exact test (comparison between LjCEP1 and mock within the same genotype). (E to G) Relative

expression level of miR2111 [(E) and (F)], LjCEPD1 (E), TML (F), and LjCEP1 (G) in different tissues under mock (water) or 1 μ M LjCEP1 treatment by quantitative reverse transcription polymerase chain reaction (qRT-PCR). Representative results from two independent experiments. (H) Under low-N conditions, CS in the root susceptible zone (SZ) is required to induce N starvation signal (CEP1) expression by an unknown mechanism to activate CRA2 in the shoots. Activated CRA2 leads to expression of CEPD1 and synthesis of miR2111. The latter moves to the roots and represses TML in the SZ, priming the uninfected roots for nodule formation. For bar plots, the error bars represent SDs. Statistical differences in (E) to (G) were determined by a two-sided Student's t test. The number of biological replicates is indicated on the graph. Scale bars, 1 mm (A) and 2 mm (C).

a paler coloration when compared with Gifu (fig. S3, C to E). Consistent with delayed development, nodules of the CS mutants also had reduced nitrogen-fixation capability (fig. S3F), despite showing no defects in bacterial colonization or abundance within the few mature nodules that occasionally formed (fig. S3, G and H). Taken together, nodule initiation, development, and function are negatively affected by the lack of a functional CS in the endodermis.

Spot inoculation with rhizobia directly on the susceptible zone induced cell divisions in Gifu and all mutant roots at 3 dpi. However, these divisions were mostly aborted in CS mutants, resulting in only a few nodules formed by 14 dpi (Fig. 2, D to F). A time-resolved whole-transcriptome analysis of spot-inoculated Gifu and CS-defective roots (0, 1, 3, and 5 dpi) revealed that the developmental stage of nodule primordia had a stronger effect on the transcriptome compared with CS presence (fig. S4A). However, at individual time points, Gifu and the CS-defective mutants exhibited distinct transcriptional responses (fig. S4B). The functions “response to symbiont” and “nodulation” were significantly enriched among the down-regulated genes in the CS-defective mutants (data S1 and S2). Moreover, genes that positively regulate nodulation (e.g., *NFR1*, *NFR5*, *CCAMK*, *NIN*, and *NF-YA1*) were repressed at 3 dpi and/or 5 dpi (fig. S4D and data S1 and S2) (25). Additionally, functions related to “nuclear division” as well as auxin and cytokinin homeostasis were also among the genes with reduced expression (fig. S4, C and D, and data S1 and S2). Given the well-established functions of auxin and cytokinin in cell division and development, we propose that, beyond infection defects, CS mutants display hormone-related transcriptional disturbances during the progression of nodule formation, which may underlie the observed developmental arrest.

CS function is coupled to long-distance signaling through CEP1

Our transcriptome analysis further revealed that the central AON player *TML* (5) was significantly up-regulated (FDR-adjusted $P < 0.05$) in axenic CS-defective roots (fig. S2B). This up-regulation also occurred in the susceptible zone of mutant roots before inoculation (0 dpi) (fig. S4E). Because apoplastic barrier mutants often exhibit changes in nutrient distribution (14, 26), and *TML* transcript levels can be induced by the presence of even low amounts of N (27, 28), we investigated whether the nodulation delay was caused by a disturbance in N homeostasis. N-related responses include a clear transcriptional up-regulation of the assimilatory machinery responsible for incorporating N into amino acids (29). Although the expression of several of these genes [e.g., *GLUTAMINE SYNTHETASE*

(*GS*) and *ASPARAGINE SYNTHETASE* (*AS*)] was significantly changed in our root transcriptome analysis, these responses were inconsistent between CS mutants—lowly expressed or absent in shoots (fig. S5, A to C). This proposes that only minimal changes in N assimilation occurred in the CS mutants under our growth conditions and as a consequence, that CS disturbance only incurred minor effects on N homeostasis. In support of this, no consistent barrier-related changes in N levels were detected in the shoots and roots under axenic conditions, whereas Gifu shoots displayed a higher N content compared with CS-defective mutants under inoculated conditions (fig. S5D), consistent with the establishment of N-fixing nodules.

In *Arabidopsis*, the CS machinery is linked to systemic N signaling (4). Therefore, we further investigated whether disruption of systemic signaling in the *Lotus* CS mutants may underlie the observed *TML* misregulation. To address this, we created homozygous crosses between the hypernodulating *tml-5* KO mutant (11) and *Ljmyb36-2* or *Ljsgn3-2* [double knockout (dKO)]. Similar to the *tml-5* single mutant, these dKO lines exhibited increased and earlier nodulation, despite containing dysfunctional CS (Fig. 3, A and B, and fig. S6, A to C). Thus, the reduced nodulation in CS mutants likely results from altered *TML* abundance. Both *tml-5* and dKO mutants displayed lower N levels in symbiont-inoculated shoots compared with Gifu (fig. S5D), likely owing to the smaller nodules. Element profiling of shoots revealed significant differences between Gifu and CS-defective mutants as well as between single CS mutants and their respective dKOs under both axenic and inoculated conditions (fig. S7). However, potassium (K) was the only element consistently depleted across all barrier-defective mutants under both conditions (fig. S7). This likely reflects a general K-retention defect, as typically seen in *Arabidopsis* CS mutants (26).

In *Medicago*, CEP1 peptides systemically repress *TML* expression (10). To test whether this applies to *Lotus* and to measure whether changes in CEP1 accumulation contribute to reduced nodulation, we applied exogenous LjCEP1 peptides (30) to the roots of the CS mutants. This induced earlier nodulation and significantly increased nodule number, independently of barrier restoration (Fig. 3, C and D, and fig. S8, A and B). A similar effect was observed when LjCEP1 was directly applied to mutant shoots (fig. S8C), which suggests that, similar to *Medicago*, LjCEP1 moves from roots to shoots to trigger downward signals that promote nodulation. In support of a role of the CS in this process, under axenic conditions, miR2111 abundance was significantly reduced in *Ljmyb36-2* shoots and the susceptible zone, whereas *TML* expression was increased in the susceptible zone when compared with Gifu (Fig. 3, E and F). This is likely because of re-

duced LjCEP1 expression in *Ljmyb36-2* roots (Fig. 3G). Supporting this, *LjCEP1*, a gene activated by CEP1 in shoots (10), was also reduced in *Ljmyb36-2* shoots (Fig. 3E). Moreover, exogenous LjCEP1 application to the roots significantly increased *LjCEP1* expression in both Gifu and *Ljmyb36-2* shoots (Fig. 3E), further increased miR2111 levels, and repressed *TML* expression in *Ljmyb36-2* susceptible zones (Fig. 3F). The earlier nodulation in *Ljmyb36-2xtml-5* dKO could not be attributed to the complementation of *LjCEP1* expression levels (fig. S8D). Taken together, we propose that in *Lotus*, CS disruption leads to diminished expression of *LjCEP1*, which delays nodulation by affecting systemic root-shoot signaling (Fig. 3H). This was further supported by ectopic expression of *LjCEP1* in the stele (31) (fig. S8, E and F), which led to significantly increased nodule occurrence in both *Ljmyb36-2* and *Ljsgn3-2* roots (fig. S8, G and H).

The nodule vascular endodermis shares a genetic CS network with roots

Besides the roots, our promoter-GUS reporter lines showed that *LjMYB36*, *LjSGN1*, and *LjSGN3* are also transcriptionally active in the nodule vascular endodermis of mature nodules (21 dpi) (Fig. 4, A and B, and fig. S9, A to G). Transmission electron microscopy confirmed that a CS is formed in the nodule vascular endodermis of Gifu at this stage, but this was not visible in *Ljmyb36-2* (Fig. 4C and fig. S10, E and F). In *Ljsgn1-2* and *Ljsgn3-2*, CS formation was sporadic between most nodule vascular endodermal cells (fig. S10, A, B, G, and H). To assess whether a functional apoplastic barrier was formed, we incubated nodules in propidium iodide solution in a similar manner as for roots. Although Gifu-derived nodules blocked propidium iodide penetration into the xylem, all tested mutants showed increased fluorescence in the nodule vascular endodermal cell walls and in the xylem (Fig. 4, D and E, and fig. S10, C and D), consistent with diffusion into the stele. Thus, *LjMYB36*, *LjSGN1*, and *LjSGN3* are essential for functional CS formation in the nodule vascular endodermis.

Nodule vascular barriers are required for ion and metabolic homeostasis

In line with the lack of apoplastic blockage, mature CS-deficient nodules displayed significantly higher levels of sodium (Na), phosphorus (P), K, and molybdenum (Mo) compared with nodules from Gifu plants (Fig. 4F and fig. S11A). Despite this, the distribution of Na and P remained unchanged across the nodule (fig. S11, B and C). Similarly, iron (Fe) distribution was unaffected (fig. S11D). In Gifu, K was evenly distributed from the nodule vasculature to the nodule center, whereas in mutants, this was skewed toward the nodule center (fig. S11E). Mo levels gradually increased from the nodule

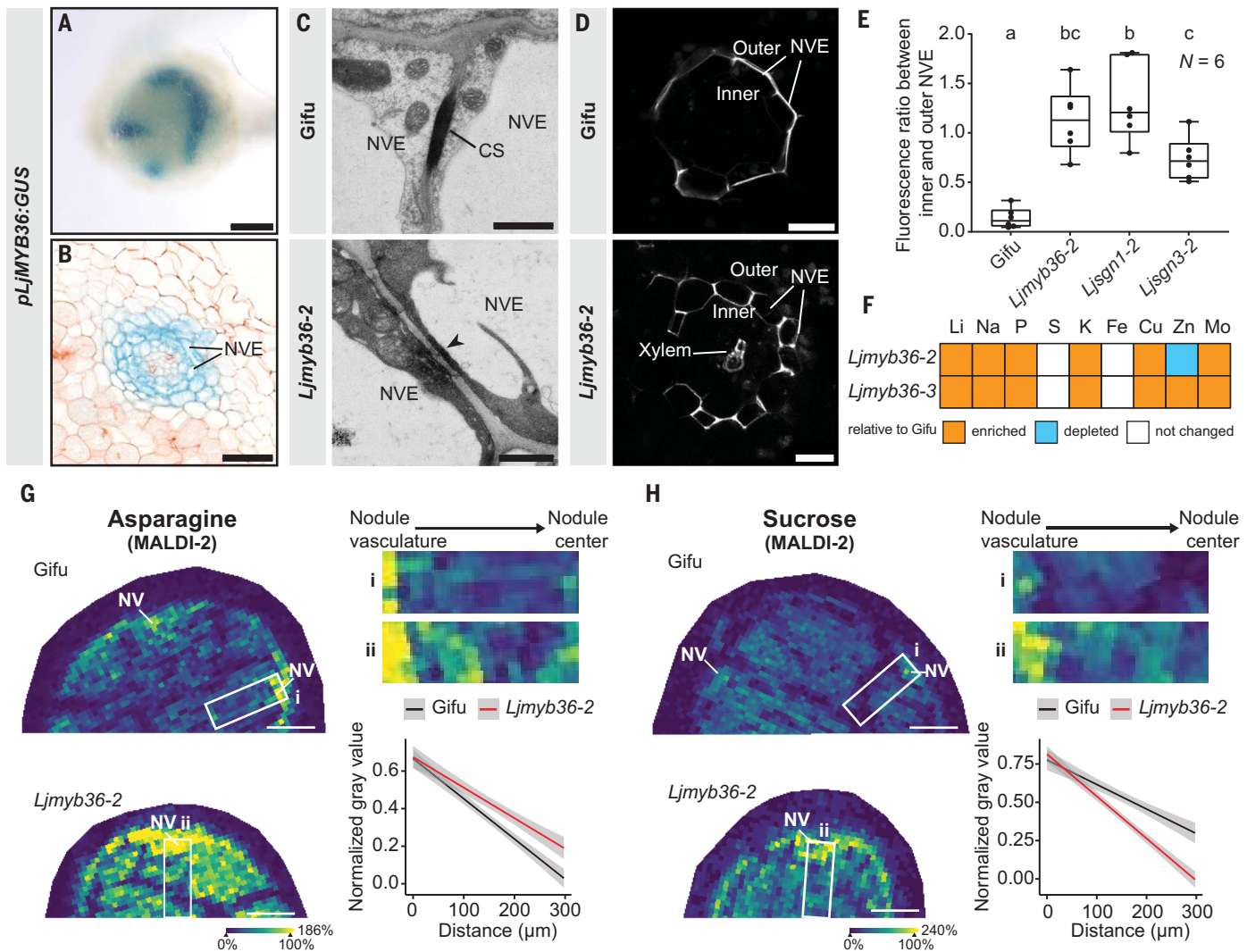


Fig. 4. Disturbed nodule function in nodules of CS-defective mutants.

(A and B) Transcriptional activity of *LjMYB36* in mature nodule at 21 dpi. Representative images of at least 15 nodules from individual plants. (C) Transmission electron microscopy images of two nodule vascular endodermal cells at 21 dpi. Electron-dense depositions highlighted by a line represent CS in Gifu nodule vascular endodermis (NVE). Arrowhead indicates the absence of CS in *Ljmyb36-2* NVE. Representative images of at least five nodules from individual plants. (D) NVE stained with PI dye (white signal). Representative images of at least 10 nodules from individual plants. (E) Quantification of fluorescence signals between inner and outer NVE. Different letters indicate statistically significant differences in a one-way ANOVA analysis with Tukey's test ($P < 0.05$). (F) Heatmap of element contents in *Ljmyb36* nodules relative to Gifu (orange, enriched; blue,

depleted; white, not changed). Statistical differences were determined by a two-sided Student's *t* test. (G and H) Distribution patterns of asparagine (G) and sucrose (H) from nodule vasculature (NV) to the nodule center at 21 dpi, detected by microsatellite instability (MSI) analysis in negative mode with postionization (MALDI-2). Line indicates a smoothed conditional mean of three biological replicates using linear model method. Shade indicates 95% confidence interval. See two additional biological replicates in fig. S14. For boxplots, the center line in the box indicates the median, dots represent individual data points, the box limits represent the upper and lower quartiles, and the whiskers represent the maximum and minimum values. The number of biological replicates is indicated on the graph. Scale bars, 250 μm (A), 50 μm (B), 1 μm (C), 20 μm (D), and 200 μm [(G) and (H)].

vasculature to the center in Gifu, but in CS mutants, Mo was more enriched in the nodule vasculature and periphery (fig. S11F). Because rhizobial distribution and abundance within nodules were unaffected in the CS-defective mutants (fig. S3H and fig. S11G), we conclude that one role of the CS in the nodule vascular endodermis is to facilitate control over element homeostasis by restricting diffusion in the apoplast.

To explore how altered element distribution affects nodule-residing bacteria, we conducted a meta-transcriptome analysis of mature Gifu and *Ljmyb36-2* nodules. Transcriptional profiles of both symbiont and host separated into distinct clusters determined by the host genotype (fig. S12, A and B), which indicates that the absence of a functional CS in the nodule vascular endodermis affects the transcriptional responses in both the host tissue and bacteria.

Genes essential for nitrogen fixation (32–34) were unchanged in *Ljmyb36-2* nodules (fig. S12, C and D), consistent with unaltered protein abundance (fig. S12E). However, several Nod factor biosynthesis genes were down-regulated in rhizobia within *Ljmyb36-2* nodules (FDR-adjusted $P < 0.05$) (fig. S12C), which suggests changes in the bacterial-host interaction. In line with this, “extracellular structures” and “cell motility” functions were enriched in

up-regulated bacterial genes (FDR-adjusted $P < 0.05$) of *Ljmyb36-2* (fig. S12F and data S2). Because these functions are typically repressed during the transition from free-living bacteria to N-fixing bacteroids (35), nodule-residing bacteria might be less genetically differentiated in mutants or display other related differences.

Among the plant differentially expressed genes, CS-related genes (e.g., *LjCASP*s and *LjESBI*) were down-regulated in *Ljmyb36-2* nodules (fig. S12D and data S1). Moreover, these also displayed a significant repression of N fixation-relevant metabolic pathways, including “asparagine biosynthetic process” and “starch and sucrose metabolism” (fig. S12G and data S2). In *Lotus* nodules, reduced N (in the form of NH_4^+) is added to glutamate to produce glutamine by GS and converted to asparagine by AS (36) (fig. S13A). The two highest-expressed asparagine synthases in nodules, *LjAS1* and *LjAS2*, were down-regulated, whereas the two highest-expressed asparaginases (converting asparagine to aspartic acid), *LjNSE1* and *LjNSE2*, were up-regulated in *Ljmyb36-2* nodules (fig. S13, A and B). Because none of the investigated genes showed altered expression in young, developing nodules (14 dpi) (fig. S13C), N metabolism defects likely arise in mature nodules owing to the CS dysfunction. The underlying cause is likely a perturbation of the source-sink relationship between the vasculature and the nodule proper. Thus, disrupted photosynthate metabolism may lead to fixed N being shuffled into aspartate rather than exported out of the nodule. In support of this, glutamine and aspartate levels were significantly increased in mature *Ljmyb36* nodules (fig. S13D), and although the level remained unchanged, asparagine distribution across the nodule was altered (Fig. 4G, fig. S13D, and fig. S14A). Moreover, in further support of a changed source-sink relationship, sucrose accumulation was increased in mutant nodules (fig. S14B) and showed preferential distribution toward the nodule periphery and vasculature (Fig. 4H and fig. S14C). Combined, these findings support that in nodules, the CS is not only required for apoplastic control of nutrient diffusion but also plays an essential role in source-sink-determined metabolic equilibria between plants and bacteria, which serves to ensure optimal N fixation.

Discussion

CS formation in the root endodermis is a fundamental prerequisite for selective ion uptake, supporting efficient long-distance transport in the vasculature of most plants (*T*). Symbiotic relationships with microorganisms pre-date vascular development and its barriers (37). Emerging evidence suggests that barrier establishment pathways are intertwined with biotic and nutritional integration in soil environments (4); yet, a direct mechanistic connection between barrier function and sym-

biosis remains unknown. Our findings illustrate that CS is essential for efficient nodule establishment and, in mature nodules, serves as an apoplastic barrier to sustain metabolic upkeep for a spatially restricted mutualism.

CS formation machinery links to systemic N signaling in *Arabidopsis* (4). In this work, we provide evidence that in *Lotus*, the CS is implicated in systemic signaling to regulate AON under low-N conditions. However, whether the relationship between CS and *LjCEP1* expression is direct or indirect remains unclear. CS is critical for nutrient uptake capacity and helps to retain signals within the stele, and CS-defective roots may allow long-distance signaling peptides, such as *LjCEP1* (and in *Arabidopsis*, possibly *AtCEP1*) peptides, to diffuse from the stele, exacerbating root-shoot miscommunication. Nonetheless, such effects would likely affect all peptide-based root-shoot signaling through the vasculature. CS disruption also affects nutrient distribution dynamics. Therefore, although the overall N levels were unaffected in CS mutants under N-limited conditions, spatial distribution or flow dynamics of N could be altered.

Barriers in the nodule periphery control oxygen permeation into nodule tissue (38). Defective mutants of such barriers have increased oxygen levels within nodules and reduced nitrogenase activity. This highlights that compartmentalization not only occurs in the symbiosome (i.e., intracellular bacteria surrounded by peribacteroid membrane) (39) but also in other nodule tissues by forming physical barriers for proper nodule function. The CS also plays an important role in exudation that shapes the rhizosphere-associated microbial communities (40). Thus, our mutants with CS-deficient nodules also represent a model to compare nodules with rhizosphere communities and investigate how compound exchanges influence free and constrained plant-microbe associations.

REFERENCES AND NOTES

- N. Geldner, *Annu. Rev. Plant Biol.* **64**, 531–558 (2013).
- T. G. Andersen et al., *Curr. Biol.* **31**, 965–977.e5 (2021).
- R. Heidstra et al., *Plant Physiol.* **105**, 787–797 (1994).
- D. Shen et al., *EMBO J.* **43**, 2486–2505 (2024).
- P. Gautrat, C. Laffont, F. Frugier, S. Ruffel, *Trends Plant Sci.* **26**, 392–406 (2021).
- C. Laffont, F. Frugier, *New Phytol.* **241**, 24–27 (2024).
- N. Imin, N. A. Mohd-Radzman, H. A. Ogilvie, M. A. Djordjevic, *J. Exp. Bot.* **64**, 5395–5409 (2013).
- N. A. Mohd-Radzman et al., *Plant Physiol.* **171**, 2536–2548 (2016).
- C. Laffont et al., *Plant Physiol.* **180**, 559–570 (2019).
- P. Gautrat, C. Laffont, F. Frugier, *Curr. Biol.* **30**, 1339–1345.e3 (2020).
- D. Tsikou et al., *Science* **362**, 233–236 (2018).
- T. T. Xiao et al., *Development* **141**, 3517–3528 (2014).
- K. Hartmann, E. Peiter, K. Koch, S. Schubert, L. Schreiber, *Planta* **215**, 14–25 (2002).
- T. Kamiya et al., *Proc. Natl. Acad. Sci. U.S.A.* **112**, 10533–10538 (2015).
- L. M. Liberman, E. E. Sparks, M. A. Moreno-Risueno, J. J. Petricka, P. N. Benfey, *Proc. Natl. Acad. Sci. U.S.A.* **112**, 12099–12104 (2015).
- V. G. Doblaz et al., *Science* **355**, 280–284 (2017).
- T. Nakayama et al., *Science* **355**, 284–286 (2017).
- J. Allassimone et al., *Nat. Plants* **2**, 16113 (2016).
- T. Mun, A. Bachmann, V. Gupta, J. Stougaard, S. U. Andersen, *Sci. Rep.* **6**, 39447 (2016).

- A. Matolepszy et al., *Plant J.* **88**, 306–317 (2016).
- R. Tsumamoto, H. Fukuoka, Y. Takahata, *Plant J.* **54**, 30–42 (2008).
- J. Allassimone, S. Naseer, N. Geldner, *Proc. Natl. Acad. Sci. U.S.A.* **107**, 5214–5219 (2010).
- D. Roppolo et al., *Nature* **473**, 380–383 (2011).
- P. S. Hosmani et al., *Proc. Natl. Acad. Sci. U.S.A.* **110**, 14498–14503 (2013).
- S. Roy et al., *Plant Cell* **32**, 15–41 (2020).
- A. Pfister et al., *eLife* **3**, e03115 (2014).
- M. Sexauer et al., *Nat. Commun.* **14**, 8083 (2023).
- M. Hayashi-Tsugane, M. Kawaguchi, *Planta* **255**, 95 (2022).
- J. Swift, J. M. Alvarez, V. Arous, R. A. Gutiérrez, G. M. Coruzzi, *Proc. Natl. Acad. Sci. U.S.A.* **117**, 12531–12540 (2020).
- J. Lin, Y. P. Roswanjaya, W. Kohlen, J. Stougaard, D. Reid, *Nat. Commun.* **12**, 6544 (2021).
- W. Dong et al., *Nature* **589**, 586–590 (2021).
- J. T. Sullivan, S. D. Brown, C. W. Ronson, *PLOS ONE* **8**, e53762 (2013).
- L. Wang et al., *New Phytol.* **224**, 818–832 (2019).
- T. Ott et al., *Curr. Biol.* **15**, 531–535 (2005).
- R. Ledermann, C. C. M. Schulte, P. S. Poole, *J. Bacteriol.* **203**, e0053920 (2021).
- L. Wang et al., *Plant Biotechnol. J.* **20**, 616–618 (2022).
- M. K. Rich et al., *Science* **372**, 864–868 (2021).
- R. E. Venado et al., *Proc. Natl. Acad. Sci. U.S.A.* **119**, e220629119 (2022).
- N. A. Mohd-Radzman, C. Drapek, *Plant Cell Environ.* **46**, 2998–3011 (2023).
- J. Durr et al., *Plant Cell Physiol.* **62**, 248–261 (2021).

ACKNOWLEDGMENTS

The authors thank T. Timmers and the Central Microscopy facility (CeMic) at the Max Planck Institute for Plant Breeding Research (MPIPZ) for microscopy aid; A. Stamatakis and the greenhouse team at MPIPZ for help with plant growth; N. Dyballa-Rukes, S. Ambrosius, M. Grusch, and M. Graf for technical support; the Biocenter MS Platform Cologne for the inductively coupled plasma mass spectrometry measurements; and the CEPLAS Plant Metabolism and Metabolomics Laboratory for total N measurements. K. Markmann and M. Sexauer are thanked for sharing protocols, *tnl-5* seeds, and constructive discussions. T. Zeng and C. Gütjahr are thanked for sharing protocols. K. Hlaváčková is thanked for help with experiments. Moreover, we thank N. Geldner, J. Vermeer, R. Ursache, G. Reyt, M. Marek, and S. Fujita for insightful discussions. B. De Rybel and A. P. Mähönen are also thanked. **Funding:** This study received funding from the Sojka Kovalevskaja program at the Alexander von Humboldt foundation (T.G.A.); the Max Planck Society (T.G.A.); the German Academic Exchange Service (DAAD, Graduate School Scholarship Program reference no. 91713467) (R.E.V.); German Research Foundation, DFG grant MA 7269/1-1 (M.M.A.); Deutsche Forschungsgemeinschaft (DFG, German Research Foundation) under Germany's Excellence Strategy – EXC-2048/1 – project ID 390686111 (T.G.A., S.K., P.W., S.M., and S.S.); Novo Nordisk Foundation grant NNF220C0075787 (N.B.); and Carlsberg Foundation grant CF21-0498 (N.B.). **Author contributions:** Conceptualization: D.S., T.G.A.; Funding acquisition: T.G.A.; Investigation: D.S., S.S., N.M., R.E.V., C.C., D.P.P., U.N., R.T.N.; Methodology: D.S., N.M., R.E.V., N.B., C.C., D.P.P., S.M., P.W., S.K., U.N., R.T.N., M.M.A., T.G.A.; Project administration: T.G.A.; Supervision: T.G.A.; Visualization: D.S., T.G.A.; Writing – original draft: D.S., T.G.A.; Writing – review & editing: all authors. **Competing interests:** The authors declare that they have no competing interests. **Data and materials availability:** All data are available in the main text and the supplementary materials. Newly created materials are accessible from the corresponding author upon request. RNA sequencing raw reads generated in this study have been deposited at the National Center for Biotechnology Information under BioProject IDs PRJNA1022778 (nodule primordia and mature nodules) and PRJNA1022988 (axenic roots). **License information:** Copyright © 2025 the authors, some rights reserved; exclusive licensee American Association for the Advancement of Science. No claim to original US government works. <https://www.science.org/about/science-licenses-journal-article-reuse>

SUPPLEMENTARY MATERIALS

[science.org/doi/10.1126/science.ado8680](https://www.science.org/doi/10.1126/science.ado8680)
Materials and Methods
Figs. S1 to S14
Tables S1 to S4
References (41–70)
MDAR Reproducibility Checklist
Data S1 and S2

Submitted 24 February 2024; resubmitted 23 September 2024
Accepted 11 February 2025
10.1126/science.ado8680